Stockholm University

Bachelor Thesis

Degree Project in Marine Geology 30 hp

Upper slope sedimentation environments in the Gaoping river-sea system of SW Taiwan

Lina Hansson

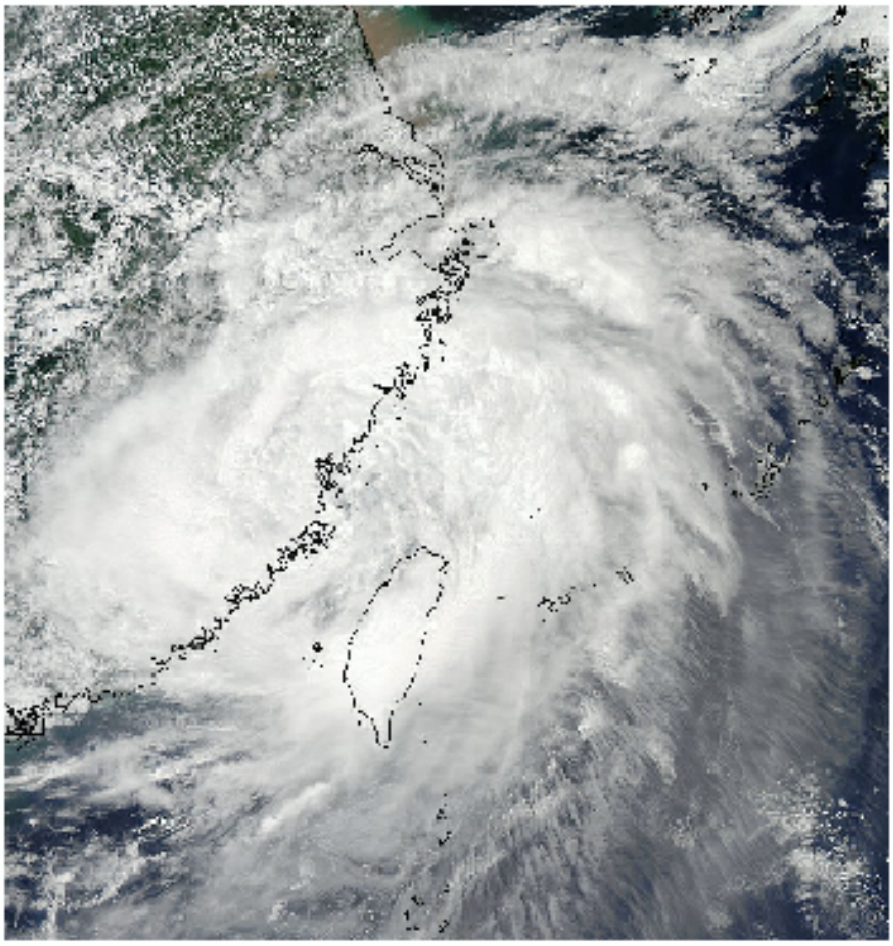

Stockholm 2013

Department of Geological Sciences
Stockholm University
SE-106 91 Stockholm

Table of Contents

Abstract 3

Introduction 4

- Background 5
  - River-Sea System 6
  - Annual changes in sediment delivery 7

Methods 9

- Marine coring 9
- Core sampling 10
- Loss on Ignition 10
- Freeze drying 10
- Grain Size 11
- Pb-210 11
  - Procedure 12
  - Calculations 13

Results 14

- 2009_L28 14
- 2010_L28 15
- 2009_L9 17
- 2010_L9 18

Discussion 20

- 2009_L28 21
- 2010_L28 22
- 2009_L9 23
- 2010_L9 24
- Two sedimentation regimes 25
- Cyclicity and monsoons 26

Conclusions 27

Acknowledgements 28

References 28

Appendix 32

Abstract

The Gaoping Slope, off the south west coast of Taiwan, is a tectonically active sedimentation environment attaining most of its sediment from the Gaoping River. This study examines sediment cores from two localities at 375 m and 495 m water depth by using X-radiography, Grain size- and ^{210}Pb analysis, with the purpose of comparing the sedimentation environment at the two sites and examine how they were both affected by high sediment delivery during typhoon Morakot.

The shallow site has coarse bioturbated sediment, whereas the deeper site had laminated fine sediment containing high amounts of organic material. Both localities display a 13-20 cm thick recently deposited layer in the cores taken after typhoon Morakot. The layers are characterized by coarsening-fining sequences. All cores show cyclicity in the grain size data.

We suggest that the shallow station has a more energetic environment, affected by wave reworking, tides, and alongshore currents supplying riverine material from the Gaoping river. The deep site has a calmer sedimentation environment dominated by hemipelagic settling of suspended material.
The recent accumulated deposits are most likely hyperpycnites from density driven hyperpycnal flows, originally caused by canyon overflows in the Gaoping- and the Kaohsiung canyon during the typhoon.
The strata found at the Gaoping slope is a result of submarine mass transport of sediment, and reflect the interaction between annual seasons and extreme events triggered by typhoons and earthquakes - eroding, transporting, and depositing sediment in the area.

Introduction

River-Sea systems have been investigated world wide, since they play a significant part in the transport of terrigenous material towards the deep ocean (Liu & Lin, 2004). The offshore area of south-western Taiwan, the Gaoping slope, is such a system - because of its high tectonic activity and high erosion rates (3-6mm/year) it is one of the most dynamic systems in the world (Dadson et al., 2003; Huh et al., 2009). Many different kinds of sedimentary processes are going on here, mainly governed by the seasonal delivery of material from the Gaoping River.

Studying the stratigraphic record of slope sediment reveals the mechanisms behind sediment transport and do not only shed light on present circumstances, but might also give a deeper understanding for basin evolution and tectonics, climate- and sea-level changes (Dadson et al., 2003; Yu et al., 2009). Investigations of the Gaoping slope area also have additional socio-economical values due to its potential of the occurrence of gas hydrates (Yu & Huang, 2006), and its sub-sea fiber optic cables (Carter et al.,2012).

The purpose of this study is to attain a better understanding of the dynamics of the Gaoping slope. The aim is to investigate how the sedimentation environment is affected by local conditions such as location and morphology, but also to see how the sedimentation environment is affected by high sediment delivery during the summer monsoon and its associated typhoons. What mechanisms are forming the strata on different parts of the slope, and how are changing conditions manifested within the sediment? What does a flood deposit look like and what is the preservation potential of the sediment?

We will do this by studying sediment cores from two localities on the Gaoping slope, taken two months (2009) and a year after (2010) a typhoon, studying structures, grain size data and the distribution of ^{210}Pb.

Date	Cruise name	Station	Longitude	Latitude	Water depth	Sampling Method	Core Length	Referred to in text as
2009-10-01	ORI 915	L28	120.1278	22.498	375m	Box corer	50 cm	2009_L28
2009-10-03	ORI 915	L9	120.3613	22.184	495m	Box corer	50 cm	2009_L9
2010-10-06	ORI 942	L28	120.1276	22.4971	375m	Gravity corer	102 cm	2010_L28
2010-10-06	ORI 942	L9	120.3612	22.1838	496m	Gravity corer	98 cm	2010_L9

***Fig. 1**. Cores collected for this study.*

Background

The island of Taiwan is situated off the coast of South east China, at the active arc-continent collision between the Philippine and the Eurasian plate (Huh et al., 2009; Liu et al., 1993). Taiwan is in a tectonically active environment; earthquakes are frequent, and plate boundary obliquity has led to the collision propagating southward (Chang et al., 2003) with annual exhumation rates of 5–7 mm (Huh et al., 2009; Dadson et al., 2003).

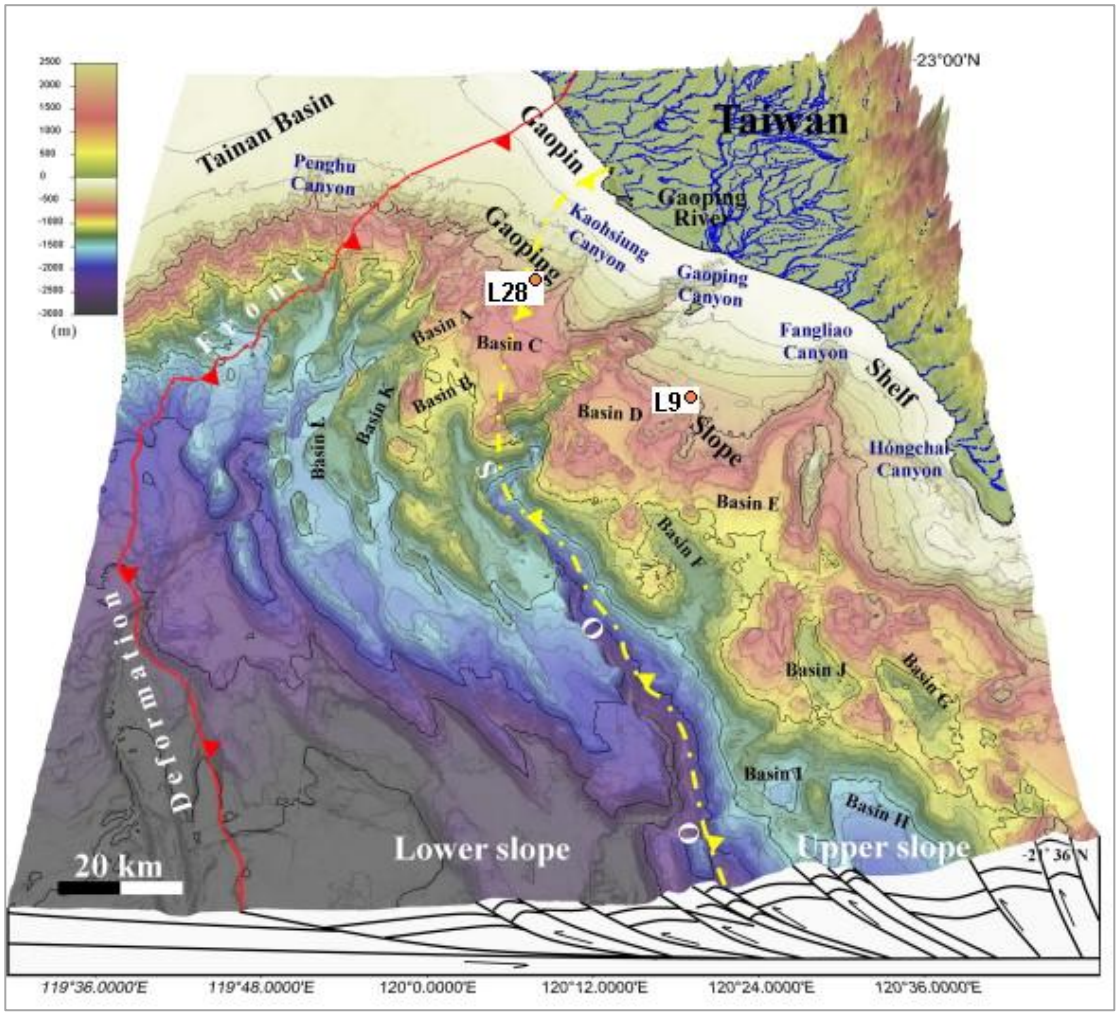

Fig. 2. *The Gaoping slope and the approximate location of the two study sites.* Modified from Huh et al., (2013)

The study area is off the south-west coast of Taiwan, and is called the Gaoping slope. It's on the propagating tip of the plate boundary, comprising an accretionary wedge that has a submarine fold-and-thrust belt along its western flank (Liu et al., 1993). Its morphology has developed from a combination of tectonic activity and its associated uplift/subsidence, and by the sedimentary processes that are active in the area. There are morphological features such as faults and folds, and

diapiric intrusions creating basins on the lower slope (Yu & Huang 2006). Three large submarine canyons, several gullies and submarine channels cut across the shelf and slope, affecting sediment transport and deposition in the area (Hsu et al., 2013).

The study sites are present in the upper slope region. Site L28 is the closest to the shore at 375 m water depth, situated close to one of the submarine canyons, Kaohsiung canyon. Site L9 is further offshore at 496 m water depth, and is situated between the two biggest submarine canyons in the area – the Gaoping- and the Fangliao submarine canyon. The sites are affected by alongshore currents and waves towards the north-west, its proximity to the submarine canyons, but also by the Gaoping River, which is the main supplier of terrestrial derived material to the area.

River-Sea System

The Gaoping River is 170 km long and consists of a system of 6 smaller rivers (Yu et al., 2009), comprising a drainage area of 3250km^2 (Huh 2009; Yu et al., 2009). The river goes through a 3952 m high mountain range consisting of highly erodible sedimentary and metamorphic rocks (Huh et al., 2009) such as sandstones, shales, and greenschist (Dadson et al., 2003; Chang et al., 2003). Consequently it carries large amounts of eroded material as it flows through the island towards the sea. Its sediment load is estimated to be from 36Mton/year (Huh et al., 2009) to 49Mton/year (Dadson et al., 2003), which is mostly delivered to the Gaoping slope during the annual summer monsoon (Liu and Lin, 2004; Liew et al., 1998).

As the Gaoping River empties in the sea, mass-movement processes become important mechanisms for sediment transport, dispersal and accumulation in the offshore area (Hsu et al., 2013). A total of 6.6 Mtons of sediment accumulates in the Gaoping Slope annually –only 20% of the total sediment load delivered by the Gaoping River, reflecting the extent and importance of sediment transporting mechanisms in the area.

	Shelf (<200m)	**Slope** (200-1000m)	**Basins** (>1000m)
Deposited sediment (%)	17	64	19

Fig. 3. *Fraction of the annual deposited sediment ending up in each system of the Gaoping Slope. Data from Huh et al., (2009).*

The amount of sediment depositing in the different systems, as listed in *Fig. 3* reflects not only the energy of the systems, but also the supply of material, which is decreasing with distance offshore (Hsu et al., 2013; Huh et al., 2009).

The shelf is an energetic system affected by wave reworking (Liu et al., 2002) and tidal currents,

keeping sediment from depositing. The system is considered to be a sediment bypass zone.
The slope is a temporary sink for arriving sediment. There is hemipelagic settling (Yu and Huang, 2006) of suspended particles, but also the occurrences of mass flows such as landslides, debris flows, and turbidity currents, as a result of high sediment loads from the Gaoping River. These mass flows have great kinetic energy, depositing and transporting material away from the slope (Yu & Huang, 2006; Yu et al., 2009; Hsu et al., 2013).

Sediment deposited in the basins spills over the shallow, healed (=filled) basins and gets trapped in the under-filled basins situated at greater depths.
If sediment is transported into a submarine canyon the sediment ends up in the deep ocean, in this case the northern parts of the Manila Trench (Yu et al., 2009). Submarine canyons are known conveyors of terrestrial sediment towards the deep ocean and have similar transport mechanisms as the slope, with failures along its walls creating slumps and debris flows, and turbidity currents with high velocities transporting the sediment down slope (Huh et al., 2009). As the Gaoping canyon is situated only 1 km off the mouth of the Gaoping River, it receives a lot of riverine material. When the sediment load of the river is high enough (36-43 kg/m^3) a *hyperpycnal flow* commonly forms (Cheng and Su, 2012; Liu et al., 2006; Liu et al., 2004; Liu et al., 2002). It is a mass-flow driven by the density difference between the fresh riverine sediment-water and the saline ocean water, and can travel hundreds of kilometers before it fades off (Carter et al., 2012; Mulder et al., 2003).
High sediment supply could also affect the slope are close to a submarine canyon, causing overflows of the canyons as the upper dilute part of turbidity currents flowing through them flows over the canyons' banks (Hünecke & Mulder, 2011). In local basins this can be the dominant depositional process (Yu and Huang 2006; Hsu et al., 2013), and has previously occurred in the Gaoping canyon (Huh et al., 2009).

Annual changes in sediment delivery

Most canyon overflows happen during the summer monsoon, the East Asian Monsoon. In Taiwan it brings a warm and wet May-October (Chang, 2004) as a consequence of moist air masses from the Indian- and Pacific Ocean reaches the fairly dry air of East Asia. Approximately 89% of the annual rainfall in southern Taiwan is precipitating during these months (Water resources agency, 2013). The increased water volume cause enhanced chemical weathering and water flow in the rivers, increasing both their energy and sediment load (Dadson et al., 2003). Liu, Lin & Hung (2006) estimated that the river discharge and sediment load of the Gaoping River are 2-3 orders of magnitude higher during June-September, when 78% of the rivers' annual discharge occurs (Liu et al., 2002).

Typhoons are associated with the monsoon season. These are tropical cyclones, storms, bringing high precipitation and strong winds over its affected area (Cheng et al., 2009; Tu et al., 2009). Typhoons have a more intense and sudden effect on sedimentation in the offshore area than the monsoon,

Typhoon name (CWB warning period)	Intensity classification* Characteristics	Accumulation rainfall in mm (duration) station	Casualties including Death and missing
MORAKOT 2009/08/5–10	Intermediate TC Traversing CMR+ SW monsoon	2855 mm (100 h) A-Li Shan	695
FLOSSIE 1969/10/1–7	Intermediate TC nearby + NE monsoon	2162 mm (120 h) An Pu	105
HERB 1996 07/29–08/01	Strong TC Traversing CMR	1987 mm (48 h) A-Li Shan	73
LYNN 1987/10/23–27	Strong TC nearby + NE monsoon	1497 mm (96 h) Chu Tze Hu	63
SINLAKU 2008/09/9–17	Strong TC Traversing CMR	1458 mm (96 h) A-Li Shan	21
ORA 1978/10/11–14	Intermediate TC nearby + NE monsoon	1434 mm (96 h) Chu Tze Hu	7
GLORIA 1963/9/8–13	Strong TC nearby + NE monsoon	1433 mm (96 h) A-Li Shan	363
NARI 2001/9/6–20	Intermediate TC Traversing CMR	1304 mm (72 h) Chu Tze Hu	104
HAITANG 2005/7/16–20	Strong TC Traversing CMR	1216 mm (72 h) A-Li Shan	15
MINDULLE 2004/06/28–07/02	Intermediate TC Traversing CMR	1182 mm (72 h) A-Li Shan	45

Fig. 4*. Record of the 10 highest typhoon accumulation rainfalls during the last 50 years.* Modified from Lin et al., 2011.
CMR: Central Mountain Range, TC: Tropical Cyclone, NE: Northeasterly, SW: Southwesterly. Strength of the typhoons are classified by maximum wind speed according to the Central Weather Bureau of Taiwan (CWB). Light: 17.2-32.6 m/s; Intermediate: 32.7-50.9 m/s;

since great amounts of sediment is deposited in a very short amount of time. Stronger typhoons commonly bring over 1000-2000 mm of rain in approximately 48-100 hours (see *Fig. 4).*The average number of typhoons was 3.3/year during 1970–99, but 5.7/year during 2000–06, due to a northward shift of the typhoon track (Tu et al., 2009).

In this study, the major importance of monsoons and typhoons is their effect on the supply of particles offshore, by increasing the water supply and energy of the Gaoping River. Two of the most recently mentioned typhoons affecting the Gaoping slope are Haitang (16-20 July, 2005) and Morakot (5-10 august 2009). Typhoon Haitang struck the area in 2005, produced over 1200 mm of

rain in 3 days, and caused oceanic floods on the Gaoping Slope (Huh et al., 2009). Typhoon Morakot produced as much as 2777 mm, and a peak river discharge of 27 444 m3/s at the mouth of the Gaoping River (Carter et al., 2012; Ge et al., 2010), causing fiber optic telecommunication cable breakages within the Gaoping Submarine Canyon (Carter et al., 2012), not only from sediment flows caused by the current itself, but also from sediment failures in the unstable deposits it created.

Methods

Marine coring

During the ORI-915 cruise a box corer was used. It consists of an open steel box that is pressed into the sediment with help from weights, and thereby traps the sediment. The top and bottom openings are sealed before it is retrieved on board (Schulz and Zabel, 2006).

Subsamples from the box core were transferred from the box before transporting it to the lab at NTU. The top 50 cm of the sediment was analyzed for this study.

A gravity corer was used for coring on the ORI-942 cruise. It consists of a steel pipe with a plastic liner inside that penetrates the sediment once reaching the ocean floor. A core catcher keeps the core from falling out of the liner (Schultz and Zabel, 2006).

The cores were taken to the National Taiwan Ocean University (NTOU) where the sediment liners were cut into 50 cm long sections and split in half with a saw. A fishing line was used to split the sediment. The top 100 cm of sediment was analyzed for this study.

X-radiography

X-radiography is used to study structures in the sediment, since structures are related to the depositional environment- and the sedimentary processes that the sediment has been subjected to.

Twentyfive centimeter long plastic containers with 1 cm high edges were pushed into the sediment, and the filled containers were separated from the core with a fishing line. An even sample surface is needed for the x-radiography to work properly.

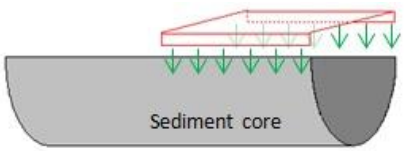

Figur 5. *Sampling the cores for X-radiography analysis.*

The core sections were put into an X-radiograph. It subjects the sample to x-rays that are either absorbed by- or go through the sediment depending on its density. The x-rays that go through the sediment are picked up by a digital imaging plate, and are black on the resulting image. Denser areas

where rays have been absorbed are white.

The image contrast was individually manipulated to facilitate distinguishing structures in them. Areas displaying the same color should therefore not be assumed to have equal density if they are present in different core sections. Also, the sections were sampled and photographed individually and there may be differences in sample thickness and instrument settings.

Core sampling

The cores were sampled every centimeter by slicing the sediment with a knife.

About 0.5-1 gram were used for grain size, and approximately 5 grams for the Pb-210 analysis.

Pb210		*Depth (cm)*	*Sampling interval (cm)*
	Marine core	0-5	2 cm
		5-100	4 cm
	Lake core	0-30	2 cm
Grain size			
	Marine core	0-100	1 cm
	Lake core	0-30	1 cm

***Fig.6**. Sampling intervals.*

Loss on Ignition

Loss on Ignition, or LOI, was done to get the organic content of the sediment. It is used for the Pb-210 analysis and is associated with organic material. The method has previously been described by Heiri et al. (2001).

Six to ten grams of (wet) sample was weighed and put into a 105° oven overnight, to let the water evaporate. Then it was weighed and put in the oven at 550° for 4 hours to combust the organic material. Finally, it was weighed again.

The LOI is calculated according to the equation:

$$LOI_{550} = ((DW_{105} – DW_{550})/DW_{105})*100$$

where DW is the dry weight after the samples has been in the oven at 105° and 500° respectively (Heiri et al., 2001).

Freeze drying

Freeze drying is a method to remove water from the sediment, which is necessairy for the Pb-210 and grain size analysis. A freeze drier freezes the sediment and then reduces the surrounding

pressure, allowing the frozen porewater to go directly from the solid phase to the gas phase (California Analytical Services).

A Kingmech model FD12-4P-D set to 30 millitorr for 70 hours was used in this study.

Grain Size

The grain size distribution in the cores allows for estimating the energy of the sedimentation environment and/or source area.

The analysis requires the removal of interfering substances such as salt, biogenic carbonates, and organic material, and has previously been described by Liu and Lin (2004).

First, the sample was washed with 15 ml RO-water (reverse osmosis water) using a Barnstead/Thermolyne (model M37615), and a Universal 32 Hettich centrifuge (type 1605-01) set to 4500 rpm for 3 minutes. This was done twice to remove salt.

Organic material was removed by adding 10 ml of 15% H_2O_2 and putting the sample in a Bransonic ultrasonic cleaner (model 5510R-MT) for 48 hours. The instrument uses ultrasound (usually from 20–400 kHz) to create cavitation bubbles that dissolve contaminants adhering to substrates (Azar, 2009). The washing procedure described above was done twice.

Then 7,5 ml of 10% HCl was added for four hours to remove carbonates. The samples were washed four times with RO-water. Lastly, to keep the grains from clustering together 7,5 ml of $Na(PO_3)_6$ was added to the samples for at least four hours.

The samples were analyzed by a Laser diffraction particle analyzer, model Beckman Coulter LS13320. It subjects the sample to a laser beam and picks up the diffraction pattern created when the light is reflected by the particles. The method is based on the principle that particles of a given size diffract light through a given angle, and with certain intensity (Cilas, 2013). The angle increases with decreasing particle size (Syvitsky, 2007)

Five measurements were made of each sample. The values were averaged and grouped into three size-classes; <4 µm (clay); 4-63 µm (silt); and 63-2000 µm (sand) according to the Udden-Wentworth US Standard (Schultz and Zabel, 2006).

Pb-210

The activity of Pb-210 can be used to determine sediment accumulation rates. It is a product of the radioactive decay of ^{238}U and has a half-life of 22.3 days (Ruiz Fernandez, 2007). The main source of lead in marine sediments is atmospheric fallout, (*unsupported* or *excess* ^{210}Pb), but it is also produced within the sediment column (*supported* ^{210}Pb) by the decay of ^{226}Ra (Appleby, 2008)

Pb-210 was determined by measuring the decay of its daughter, Po-210, with Alpha-particle Spectroscopy. This is possible since the two isotopes are in secular equilibrium with each other.

Procedure

Samples were put in plastic beakers together with some distilled water and 0.1 g of liquid Po-209 (exact amount written down for each sample). Since the instrument will pick up the decay of both Po-209 and Po-210, the measurements of Po-209 is used to calculate the efficiency of the detector. (By comparing its theoretical activity to the activity picked up by the instrument).

The beakers were put on a hot plate and a set of chemicals were added according to *Fig. 7.* to remove silicates and organic matter. The method has previously been described by Huh et al. (1987) and Huh et al. (1990). Purification of the substance is important for the alpha spectrophotometer to able to detect the alpha particles.

Chemical	**Amount**	**Wait**	**Function**
HNO_3	5 ml	30 mins	digest silicates
HF	5 ml	1 night	digest silicates
HNO_3	5 ml	30 mins	digest silicates
HF	5 ml	30 mins	digest silicates
$HClO_4$	2 ml	1 night	decompose organic matter

Fig. 7. *Chemicals used for purifying the grain size samples*

The hot plate was set to 150°C for step 1-4, and to 200° for step 5. After step 5 the lids were taken off to let the water evaporate.
Ammonia was added to separate the metallic ions from the solution. The samples were washed three times using a centrifuge set to 4500 rotations per minute for three minutes. Then 2 ml 9N HCl was added and left over night. As a last step, another 1 ml of HCl was added and the sample was immediately centrifuged for 5 minutes with 4500 rotations per minute. The remaining solution was poured into numbered glass beakers without adding any of the metallic layer located at the bottom of the tubes.

The Polonium in solution was plated onto a silver disk, which was added to the samples in the presence of ascorbic acid and distilled water, to keep the solution in a reduced environment. The vials, each covered with a lid, were put onto a hot plate (about 70-90°) for one hour. After cleaning

the silver disks with acetone and water the silver disks was counted by an Alpha counter.
The Alpha counter detects alpha particles that are emitted when radioactive isotopes decay. It produces a charge pulse proportional to each particle's energy, which is then converted to a voltage that the instrument measures (Flett Research, 2013). Each nuclide has its own characteristic energy.

Calculations

The lead from atmospheric fallout - excess ^{210}Pb - attaches to the sediment particles on the ocean floor, and continues to decay while being covered by new depositing sediment. Its activity acts as a natural clock, since the activity is related to how long the isotope has been decaying (Appleby, 2008).

To attain the excess ^{210}Pb, the activity of ^{214}Pb, an earlier lead isotope in the decay series, was used as a precursor of supported ^{210}Pb , and excess ^{210}Pb was calculated by using the equation:

$^{210}Pb_{ex} = {}^{210}Pb_{total} - {}^{214}Pb$ (Huh et al., 2009)

Sediment accumulation

Sediment accumulation is described by a steady state-advection-decay model. It assumes that the atmospheric fallout and the sediment column production of ^{210}Pb is constant, and undertakes a stable sedimentation environment with a relatively constant sedimentation rate. This is illustrated by an exponential- or quasi-exponential decrease in activity with depth (Huh et al., 2009).

The relationship between sedimentation rate and ^{210}Pb activity was earlier described by Huh et al. (1987 and 2009) using the equation:

$$^{210}Pb_{ex})_z = {}^{210}Pb_{ex})_0 \exp(-\lambda/S)$$

(where $^{210}Pb_{ex})_z$ = Activity at depth Z, $^{210}Pb_{ex})_0$ = Activity at sediment-water interface; λ = Decay constant of ^{210}Pb and S = Sedimentation rate in cm/year.
The natural logarithm of $^{210}Pb_{ex}$ was plotted against depth, and a linear regression line was drawn through the data points if suitable data was aquired. The slope of the line was then multiplied with the decay constant of ^{210}Pb (0.0311/yr) (Huh et al., 1996) to attain the sediment accumulation in cm/a (derived from the equation above).

Results

2009_L28

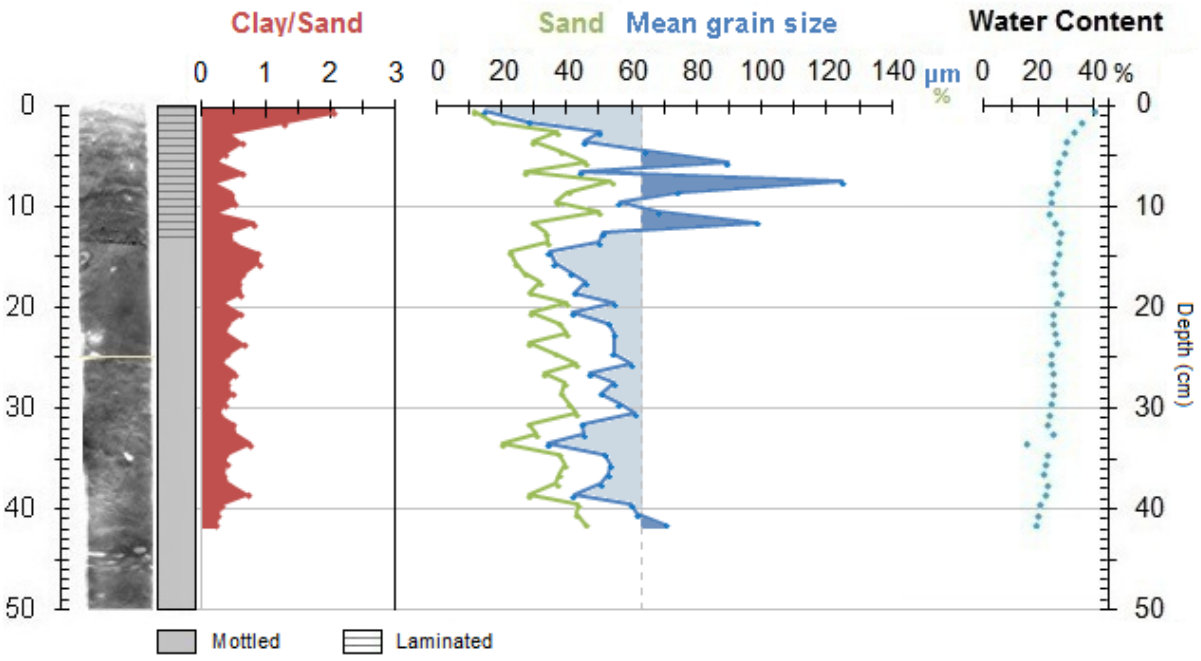

Fig. 8. *Core 2009_L28.*

Areas displaying the same color in the x-radiographic image should not be assumed to have equal density, if these areas are in different core sections.

Specific objects are only referred to if they have a diameter of 1 cm or more.

Core 2009_L28 displays a fairly homogenous mottled structure. It is laminated the top 13 cm, with cross laminations at 4.5-9 cm depth. There is a dense object at 15 cm depth and a 2 cm thick layer with horizontal oval objects at 44 cm depth.

There are two sediment types in the core; silt and sand. A mean grain size of 63 µm has been used to distinguish between the two, represented by a dotted line on *Fig. 8*). Silt is the most abundant grain size, while sand is present in the upper 4-12 cm and the last analyzed centimeter of the core.

Fluctuations in grain size are biggest the upper 13 cm, where grains range between 15-125 µm. The section is characterized by an increase in grain size down to 8 cm depth, followed by a decrease in grain size down to 15 cm. The remaining part of the core has a grain size that ranges between 34-70 µm, with a general increase in size between 15-31 cm, a decrease between 31-34cm, and another increase at 34-42 cm depth.

The grain size is highly influenced by the sand fraction which is 35% on average, but there is an

increase up to 54% at 7-8 cm depth, and a sudden drop down to 20% at 34 cm depth. Only in the upper two centimeters of the core is clay more abundant than sand.

The water content ranges between 40-15%. It decreases exponentially in the upper 10 cm, and then continues to gradually decrease with depth.

2010_L28

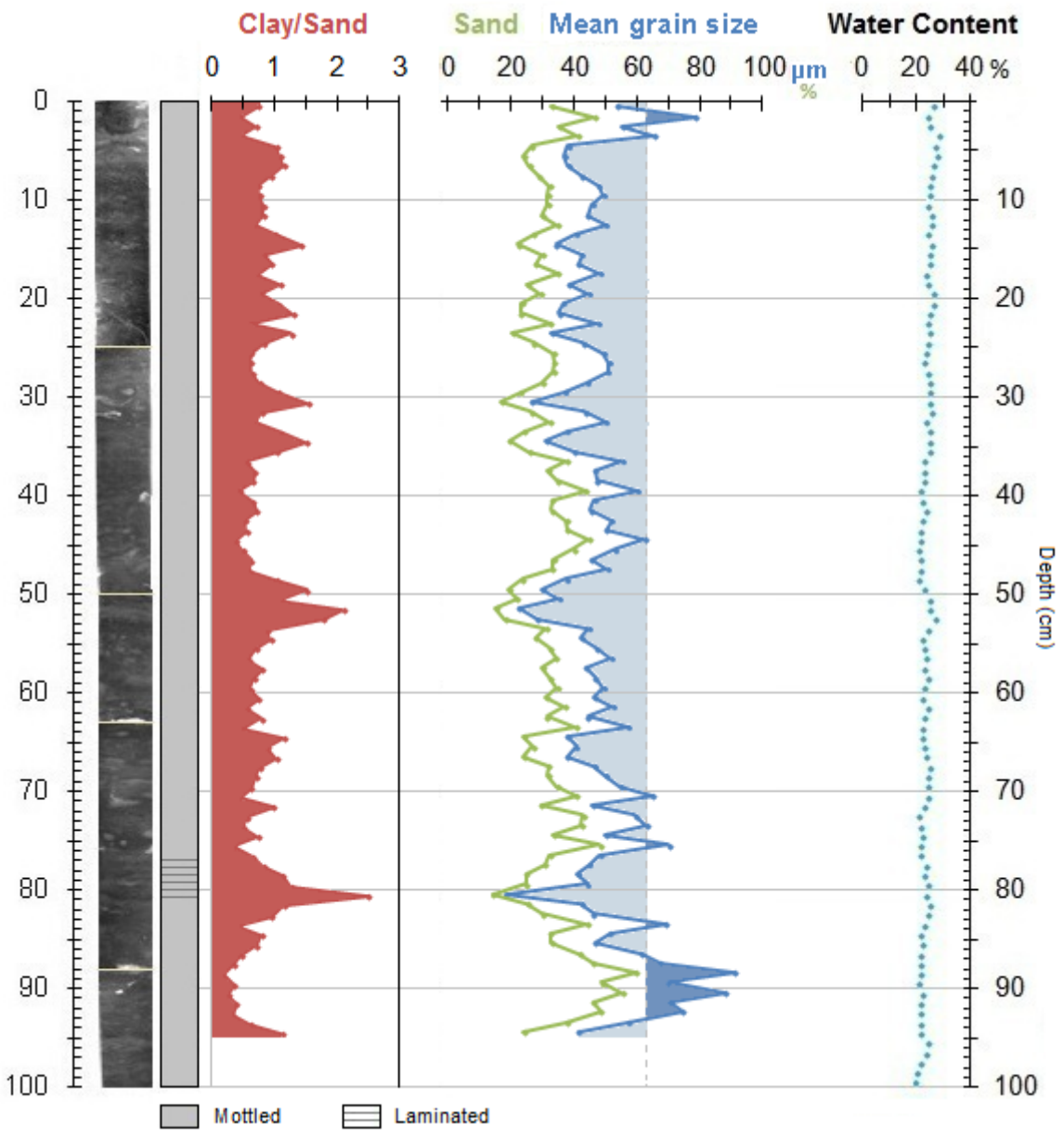

Fig. 9. *Core 2010_L28*

Core 2010_L28 is heavily mottled and has oval-and diffuse dense inclusions. Density differences show layering at 0-33 and 47-85 cm depth, and diffuse wavy laminations are present at 77-81 cm depth. The grain size is generally increasing with depth and is ranging between 18-90 µm. The sediment is

silt or sand, according to the classification method mentioned above. Sand is present in the top of the core, from 1 to 2 cm depth, but silt is the prominent grain size although it is taken over by an increasing sand content at certain depths, indicating cyclicity within the intervals 30-52cm; 52-81cm; and 81-96 cm depth. These cycles are characterized by a size increase followed by a -decrease. The deepest interval has the largest grain size variations in the core, the largest mean size, but also a significant increase in sand content, from 14% to 59% at 81 cm to 90 cm depth.

The clay:sand ratio shows a more even distribution of clay and sand in the upper 24 cm, but below this depth finer particles are generally less abundant than coarser particles, except for sudden inputs of clay; with peaks between 48-54 cm and 78-83 cm depth standing out.

The water content is between 19-28% and decreases with depth. However, the low percentage of water in the top of the core indicates that sediment might have blown off from the core, most likely during coring.

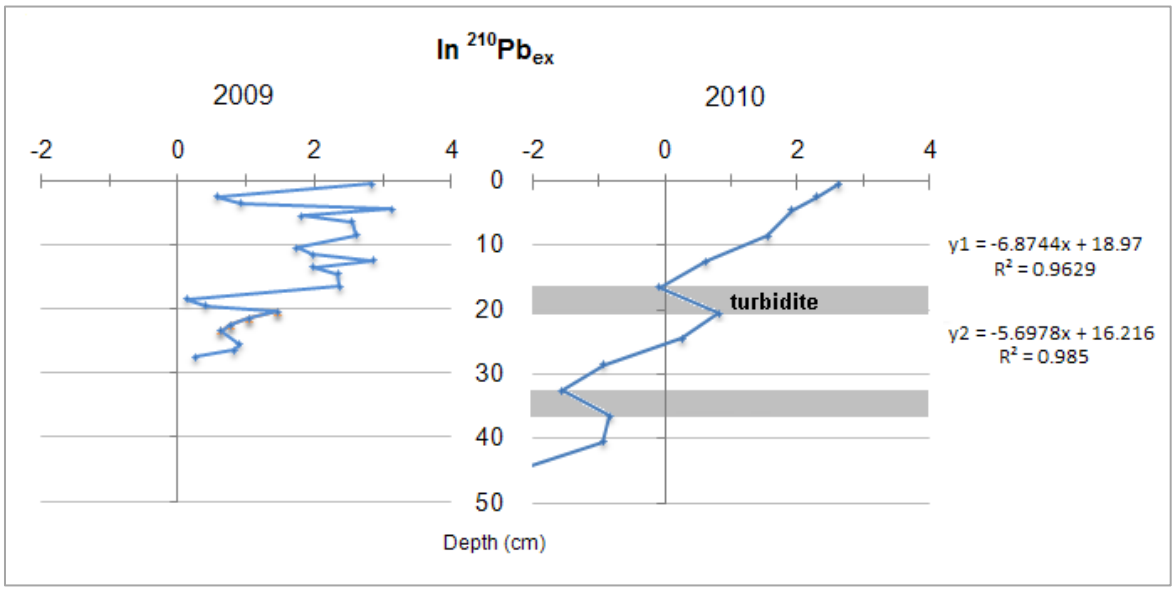

Fig. 10 *Lead profiles of cores at site L28*

The 2009 core presents a shifting lead activity, except for an abrupt decrease at 17 cm depth, and at 20-24 cm depth where a short linear decrease occurs.

The 2010 core has a linear decrease in activity at 0-18 cm and 20-32 cm depth, separated by a sudden increase in activity (a turbiditic layer) between 18-20 cm depth. Removing the turbidite layer, the sedimentation rate is 0.17cm/a or 0.21 for the 2010 core, depending on how much of the turbidite layer that is removed (the data point at 16.5 and/or 20.5 cm depth).

2009_L9

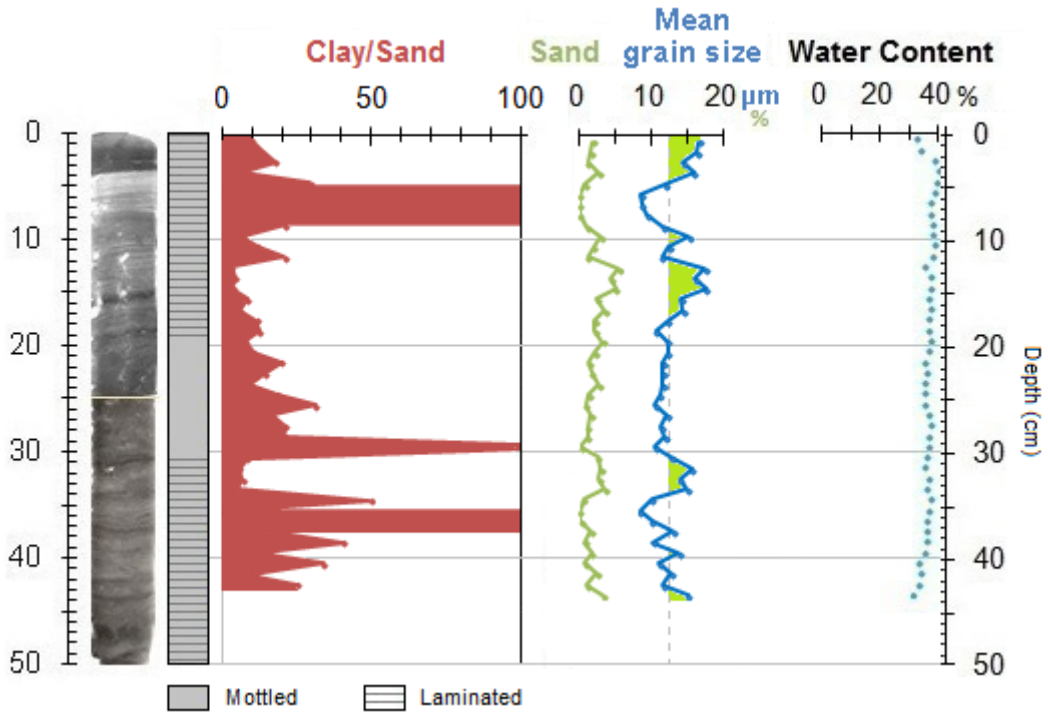

Fig. 11. *Core 2009_L9*

Core 2009_L9 is mottled and has planar, sometimes discontinuous, laminations. The upper 8 cm is characterized by a low density layer on top of a dense, laminated layer, with a sharp boundary at 4 cm depth. The laminated sediments are mottled and continue down to 19 cm depth where they are replaced by a homogenous mottled sediment, down to 31 cm depth. At 31-50 cm depth there are parallel, discontinuous laminations, and layering with diffuse boundaries.

The sediment has a fairly steady grain size. The mean size 12.6 µm is indicated by the dotted line on *Fig. 11.* Laminated sections have a fluctuating mean grain size compared to the mottled layer.

Average sand content in the core is 1.8%. Coarser intervals (in green) appear in the top 0-5; 9-13; 31-34; and 43-44 cm depth where the sand fraction is up to 2.6-5.3%.

The clay:sand ratio displays greater amounts of fine- than coarse particles throughout the core, with the highest discrepancy below 35-43 cm depth. Between 13-30 cm there is a rapid increase of the amount of fine particles with depth.

The water content is between 30-40%.

2010_L9

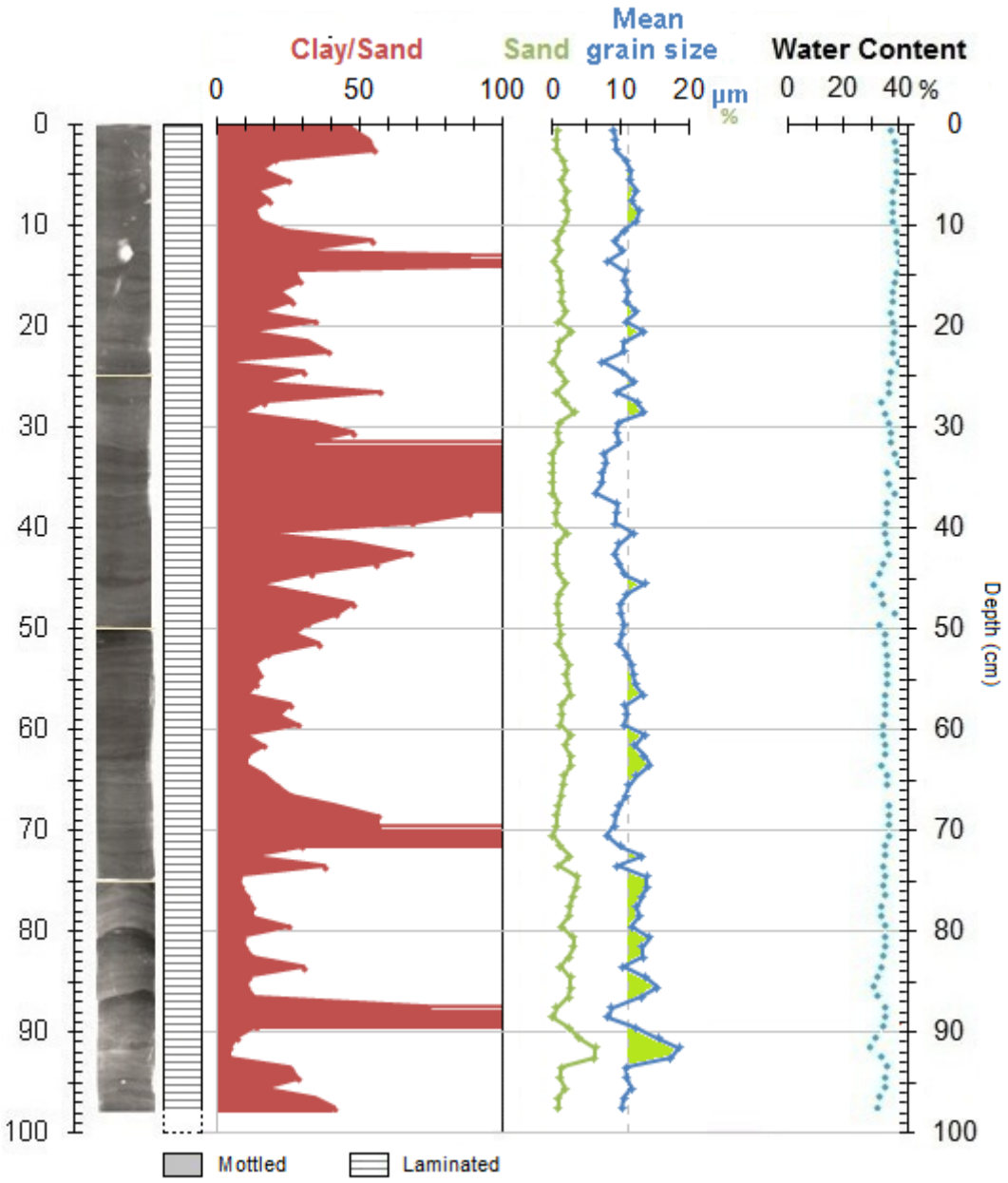

Fig. 12. *Core 2010_L9*

Core 2010_L9 display laminations and layers of different thickness that have been disturbed to some extent.

The upper 20 cm is disturbed from coring, but planar laminations of different thickness are visible.

From 20 cm down to 46 cm depth the sediment has layers and laminations of different thickness corresponding to fluctuations in grain size. These have non-parallel, somewhat wavy bedding. The layers are mottled with diffuse boundaries and are 1-4 cm thick.

The section between 46-71 cm is characterized by planar parallel- to discontinous laminations.

At 74-92 cm depth there are three sequences of ~6 cm thick layers that are separated by sharp boundaries. The layers are curved concave-down, and are characterized by a gradual density difference, although the dense part of the uppermost layer does not have the same thickness as the lower layers. There are diffuse laminations within these layers.

At 93-98 cm depth is characterized by diffuse laminations similar to the ones present in the layers described above.

The sediment has a mean grain size of 11 µm. The grain size increases with depth in the upper 10 cm. Below 10 cm depth the size is mostly between 5-15 µm. At 72-93 cm depth, there is a section with coarser mean grain sizes, containing the biggest average in the core, 18.5 µm.

The clay:sand ratio is highly changeable and corresponds to the laminations and layering in the core. From 39 cm to 64 cm the ratio is decreasing.

The sand content is 1.5% on average, but up to 6.3 % in the coarse section at 72-93 cm depth.

The water content is 30-40%.

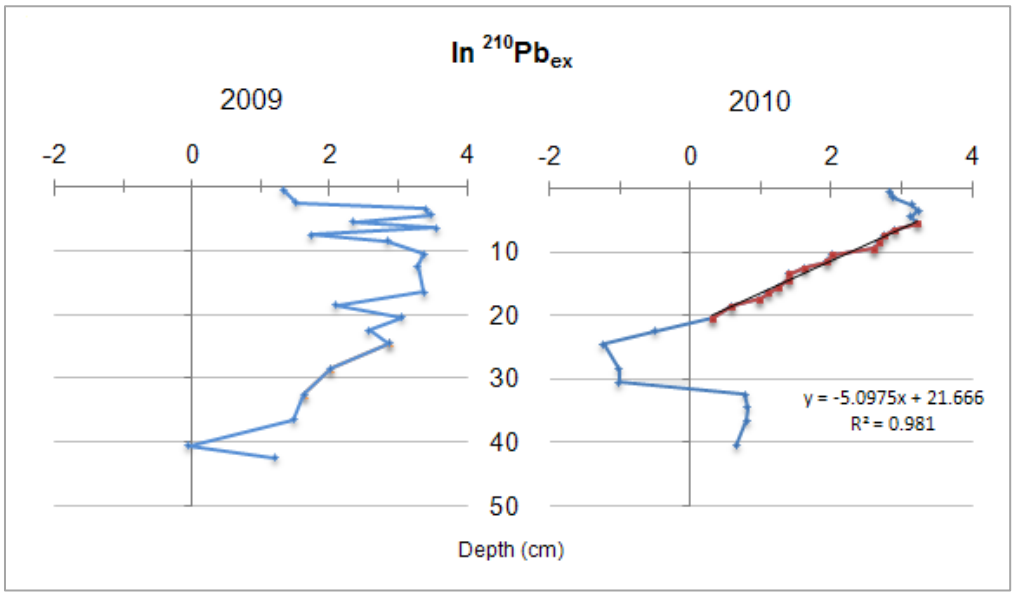

Fig. 13. *Lead profiles of cores at site L9*

The 2009 core has an increasing lead activity down to 3 cm depth, and presents varying values down to 25 cm depth. A linear decrease in activity is present at 25-32 cm.

The 2010 core has a general increase in activity the upper 5 cm. It is followed by an linear decrease in activity with depth down to 25 cm depth. After that the concentration is constant down to 31 cm depth followed by an increase between 31-33 cm depth. The value is then fairly constant down to 41 cm depth. The calculated sedimentation rate is 0.15cm/a.

Discussion

There are significant differences between the cores from the two sites, but also from different years. The different coring method has surely contributed to these dissimilarities especially in the surface sediments, but their different characteristics mainly highlight the circumstances under which the sediment was deposited. The samplings both took place during the end of a monsoon season, which are associated with high rainfall and strong chemical weathering producing great amounts of sediment which is carried offshore from the island. The strength of these monsoon seasons is the biggest reason to the observed differences in the cores from different years. The 2010 monsoon season was weak, while the 2009 monsoon season was unusually strong, bringing typhoon Morakot. Enormous amounts of sediment caused submarine floods and changed the depositional environments at the two localities, that normally have depositional environments dominated by a fairly even sediment supply, hemipelagic settling of material (site L9), wave reworking and alongshore currents (site L28) and occasional submarine failures induced by earthquakes. The enormous amounts of sediment and water eroded and redistributed already deposited material, and it is visible in our sediment cores. It is revealed that the cores from 2009 have a storm deposit the upper 13 cm (site L9) and 20 cm (site L28), lower amounts of fine grained sediment, higher fraction of coarser grains, a lack of biological activity, higher amounts of organic material, and non-steady Pb-profiles.

2009_L28

The shallow core L28 can roughly be divided into two sections; from 50 cm up to 13 cm depth the sediment has been mixed by organisms, giving it a mottled homogenous structure. The clay/sand ratio is fairly constant in this section, although the mean grain size appears to have sequences that are coarsening- and fining-up.

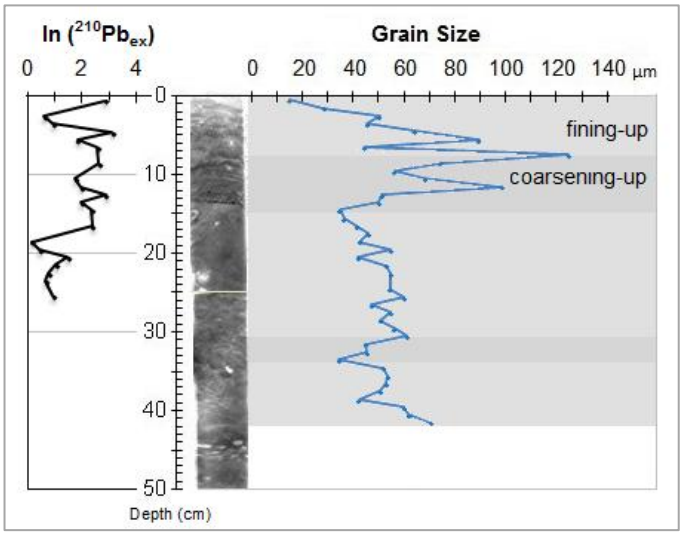

Fig. 14 *2009_L28 core.*

The upper 13 cm display discontinuous wavy laminations coinciding with great variations in grain size and high percentage of sand. There is an apparent increase- followed by a decrease in grain size, usually referred to as Ha- (coarsening-up) and Hb- (fining-up) units (*Fig. 14),* as defined by Mulder et al., (2001) and Mulder et al., (2003). The coarsening-fining sequence has most likely been created by the same event, and is a *hyperpycnite* – a deposit formed by a *hyperpycnal flow*. Grain size sequences are formed due to changes of discharge in time; the flow deposits an Ha-unit as the flood-derived sediment flow increases in strength, and an Hb-unit as the strength declines, its deposition finally being dominated by suspension fallout. The boundary between the two is at the maximum grain size and represents the maximum strength of the flow (Mulder et al., 2001), although it is not rare to have completely missing Hb-sequences resulting from erosion in energetic environments (Hüneke & Mulder, 2011; Mulder et al., 2003). Below 13 cm depth it is very likely that a similar flow has deposited the coarsening-fining sequences. The mottles indicate bioturbation which has evened out the extreme values or the hyperpycnal flows depositing the deeper sediment was simply not as energetic as the upper sequences.

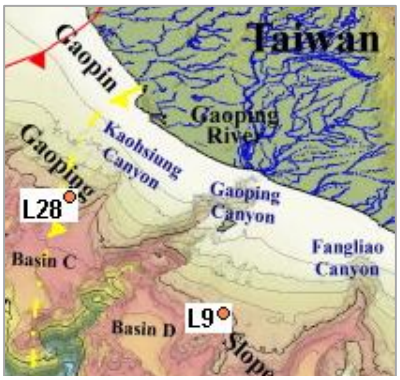

Fig. 15. *Bathymetry- and approximate location of site L28 and site L9. Modified from Hsu et al., (2013).*

Although site L28 is not adjacent to the Gaoping River, it receives riverine sediment by the north-western alongshore currents (Liu et al., 2002;), but possibly also from overflows of its neighboring submarine canyon – Kaohsiung canyon (*Fig. 15).* The Gaoping canyon had an overflow during Haitang typhoon in 2005, which was not recorded in the sediment from site L28 (Huh et al., 2009).

This is probably due to the shielding effect of the Kaohsiung canyon (*Fig. 15)* trapping the arriving flood sediment and immediately transporting it off the shelf, leaving site L28 unaffected by the flood. However, due to the significantly stronger magnitude of Morakot typhoon, the possibility of site L28 being affected by a canyon overflow is more likely than during typhoon Haitang, since Morakot possibly caused an overflow in both of the canyons (thus affecting site L28).
The deposit in the upper 13 cm could be such a flood deposit, as the lead profile has fluctuating values from 15 to possibly 20 cm depth and up, indicating that the sediment is not in a steady state, and probably newly deposited.

2010_L28

The shallow core L28 displays an altogether mottled structure. Bioturbating organisms have mixed the sediment and consumed organic material, resulting in the lowest organic content among the four cores. The core also has diffuse layering and laminations. In the lowest section (around 86-93 cm depth) and the upper four centimeters there are prominent coarser grain sizes than the rest of the core, indicating that they were deposited in a high-energy depositional environment, possibly triggered by a typhoon since they are similar to the sediment deposited by Morakot (visible in the 2009 core).

The core has a linear decrease in lead indicating a steady state environment, and has recorded a turbidite between 24-16 cm depth. Turbidites are characterized by low values of Pb_{ex}, since they erode young layers of sediment and thus expose the low activity sediment below (Liu et al., 2009). By removing the turbidite layer the sedimentation rate is 0.17/0.21 cm/a depending on how much of the section that is removed (the data point at 16.5 and/or 20.5 cm depth). This agrees well with previously determined sedimentation rates in the area which is most commonly between 0.1-1 cm/year (Huh et al., 2009).

It would be reasonable to expect newly deposited sediment, or parts of the storm deposit from 2009 in the top the 2010 core. It is very likely that these sequences have been blown off during coring, which is a common side effect to piston coring (Schultz and Zabel, 2006). That would also explain the low water content and high lead activities at the surface. There is also a possibility that the storm deposit have been eroded in situ.

2009_L9

The deep fine grained L9 core has diffuse bioturbated laminations and layers that coincide with variations of the clay/sand ratio from 50 up to 31 cm depth. At 31 cm depth homogenous sediment with a relatively constant grain size, indicates bioturbation up to 19 cm depth where the sediment continues being laminated. The obvious difference in bioturbation is likely because the organisms had sufficient time to work through the sediment.

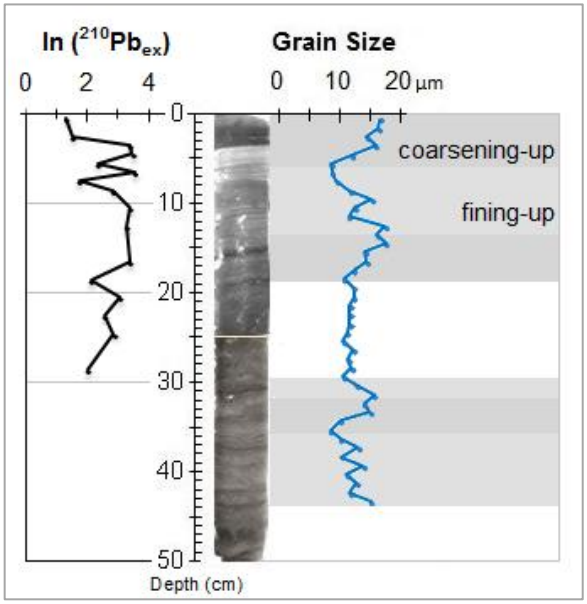

Fig. 16. *2009_L9 core.*

A clue to what processes might have formed the strata is in the upper 19 cm of the core. Here we find Hb- and Ha units (*Fig. 16*) such as in the 2009_L28 core, and the sediment deposit is thus probably a hyperpycnite. The Ha-units have parallel laminations accompanied by varying lead values (at least the upper 20 cm), and the sharp contact indicate that the flow has been so energetic it has inhibited deposition and/or eroded previously depositing sediment. This is a common feature in hyperpycnal deposits (Mulder et al., 2001).

Whether or not hyperpycnal or turbidity current flows have also formed the strata in the bottom of the core is difficult to say, but judging from the grain size distribution they are displaying similar characteristics, indicating a flood depositing coarser grain sizes at 30-34 cm depth.

As previously mentioned, site L9 is affected by overflows in the Gaoping Submarine Canyon. Huh et al. (2009) states that site L9 is present on a depositional lobe east of the canyon, made by sediment from its turbidity current overflows. The sediment has previously preserved a flood deposit induced by typhoon Haitang in 2005, characterized by exceptionally low Pb-values followed by an increase in activity which then decrease exponentially with depth. The authors concluded that these flood deposits will continue being preserved due to the thickness of the flood layer (2-12 cm depending on the location) and high sedimentation rates in its depocenter (site L9 is situated on one of the flanks) (Huh et al., 2009). There is therefore a strong possibility that there are sequences in our core originating from this, and/or a similar flood, possibly induced by the Morakot typhoon.
Our Pb-record shows that there is rapidly deposited sediment down to 20 cm depth, implying that a flood layer could be present in the fining-up-unit within this depth span. Also, the core has the highest amount of organic material of the cores, indicating fresh material being deposited.

Hyperpycnal flow deposits are associated with organic material, and frequently contain plant and wood fragments brought offshore from the continent (Hüneke & Mulder, 2011).

2010_L9

The deep L9 core has low amounts of bioturbation as indicated by the apparent laminated structure, although it is obvious that the biological activity varies. Fine grained sediment and a steady-state lead profiles reveal a sedimentation environment of a steady nature, allowing fine sediment grains to settle. There are three sequences different from the rest of the core at 72-92 cm depth, showing a gradual density difference that is fining up. The first sequence deposit, at 92-86 cm depth, has the highest percentage of sand, but the abundance seems to decrease with subsequent series.
These prominent sequences could have formed individually, from three separate sediment flows produced by three separate events, or even during the same monsoon season during periods of high rainfall. Given the obvious decrease in strength as indicated by the decreasing fraction of sand, our suggestion is that they are somehow related. Carter et al. (2012) showed how flood-induced hyperpycnal flows during a typhoon can trigger new, weaker sediment flows, when they generate unstable deposits which in turn cause new failures. The failures can be triggered by reaching a stress-threshold themselves or in a tectonically active environment like this - by earthquakes (Carter et al., 2012; Lee et al., 2009; Mulder et al., 2003). The gradual contact between the sequences indicates that the transition between the coarsening-/fining-up units has been transitional, and the flow has been too weak to completely erode previously deposited sequences (Mulder et al., 2001).

Two sedimentation regimes

	2009_L28	2010_L28	2009_L9	2010_L9
Waterdepth (m)	**375**	**375**	**495**	**496**
Structure	0-13 cm **Laminated** 13-50 cm **Mottled**	**Mottled with diffuse layering**	0-19 cm **Diffuse laminations** 19-50 cm **Mottled with diffuse layering**	**Laminated with diffuse layering**
Grain size range, µm (mean)	0-13 cm **15-125 (61.5)** 13-50 cm **35-70 (50)**	**~30-60 (48)**	0-19 cm **~8-16 (13.2)** 19-50 cm **~9-14 (12.3)**	**~ 8-12 (11)**
Sand, % (mean) maximum value	**(35) 54**	**(32) 60**	**(1.8) 5.3**	**(1.5) 6.3**
Clay/sand	**0.5 (fairly constant)**	**0.5-1.5 (a few peaks)**	**~20 (high variation)**	**~30 (high variation)**
Water, %	**20-40**	**20-30**	**30-40**	**30-40**
LOI , mean %	**3.2**	**2.8**	**3.9**	**3.6**
Pb-profile	**non-steady**	**steady**	**non-steady**	**steady**

Fig. 17. *Summary of core characteristics.*

The cores have different characteristics, highlighting the dynamics of the Gaoping slope.

The mottled structure at site L28 and the laminations and high organic content of the cores from site L9, has formed because of the difference in biological activity – it's higher at site L28. This is probably due to site L28 being closer to the shore where there is a higher supply of continent derived organic material.

There are more or less laminations present in all cores coinciding with changes in grain size, which says something about the energy of the two sedimentation environments. Grain size is strongly dependent on the flow energy of the water and sediment that reaches the ocean floor, where high energy and turbulence will deposit coarse, heavy, sediment particles, and carry the finer particles to greater depths where they can settle. Being present on the upper slope fairly close to the shore line,

site L28 has an environment dominated by wave reworking, tides, and alongshore currents enriching the coarse particles while transporting fine particles down-slope. In contrast site L9, with fine grained laminated sediment, indicates a calmer sedimentation environment, still affected by fine grained sediment overflows from the canyon in times of high sediment load.

Even if site L28 from a grain size point of view has a more energetic environment than site L9, site L9 has a lower sedimentation rate due to the lower sediment delivery.

Cyclicity and monsoons

The differences in bioturbation and grain size influence how the sediment responds to changing conditions in its environment. The sediment cores from 2010 both show cyclicity but on different scales. In core 2010_L28 the most apparent cyclicity is the clay/sand ratio peaks and grain size (at 30-34 -, 52-, 65-, and 81 cm depth) - while in the 2010-L9 core the cycles are displayed in both the laminated structure and grain size (clay/sand ratio) (at 13-, 32-38 -, 70-, and 88 cm depth) (see *Fig. 18*).

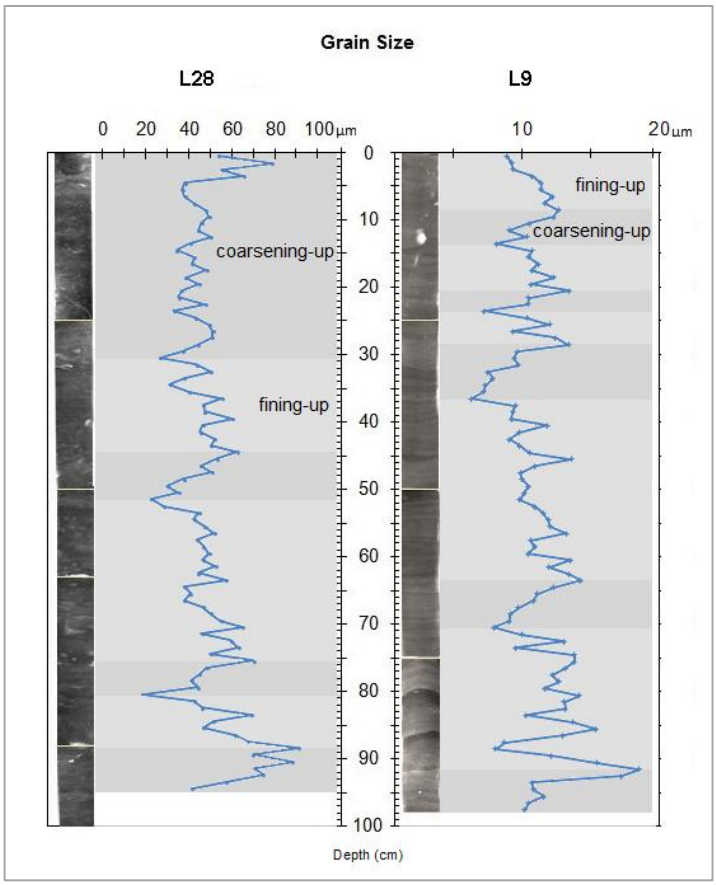

Fig. 18. *Cyclicity in the cores from 2010.*

Grain size cyclicity can be attributed to large scale climate change, such as differences in monsoon strength, variations in solar radiation, the Earth's orbit, or glacial/interglacial cycles as well as storms.

On a smaller time scale grain size is commonly interpreted as annual changes in sediment delivery. This is partly the case in our cores since the area is affected by annual monsoon seasons, and thus has a strong seasonal signal. Judging from the width of the cycles this would imply sedimentation rate of around 20cm/year on average. However, from the 2009 cores it is apparent how much impact a single typhoon can have on the stratigraphy, adding the importance of single events *during* the monsoon season. We suggest that the cyclicity is a result of the interaction between annual seasons, and extreme events triggered by typhoons and even earthquakes. These create sedimentary flows that are in turn generating unstable

deposits, and modify the sediment with their associated erosion, removing the fine particles that have been deposited by hemipelagic sedimentation. This is apparent by the low sediment accumulation rates (1-2 mm/year) knowing mass flows are common in the area.

Our cycles are jagged, which is related to the flow and frequency of the sediment flows. Especially hyperpycnal flows are “quasi-steady”, meaning that their velocity increases and decreases with time, giving them a pulsed nature (Mulder et al., 2003), which can cause intra-sequence erosion (Hüneke & Mulder, 2011). In addition, sediment from one flow can create unstable deposits once it’s settled on the ocean floor, creating failures which generate new sediment flows, as previously discussed.
Also, flows can transform. Hyperpycnal flows might transform into turbidity currents or vice versa, (Carter et al., 2012) creating interrupted sequences, disturbing previous-, and depositing new sediment.
The varying strength and dynamics of the sediment flows, also affect the cycles and their width. These are closely connected to variations in monsoon strength which varies on both a short- and long time scale (Allan, 1996; Wu et al., 2004). This is also apparent comparing our cores, taking into account the different strengths of the monsoon seasons in 2009 and 2010, and what signal they produced in the sediment.

Conclusions

Our cores show that the sedimentation environments of our localities are different.
Hemipelagic settling of suspended material depositing laminated sediment occur at site L9 where the supply of material is low, and coarser grained sediment with high bioturbation rates is accumulated where the sediment supply is higher, at site L28. The proximity to submarine canyons is a prominent factor determining the sedimentation environments, and can both have a shielding effect, ”protecting” the site from arriving sediment by transporting it offshore, and act as a supplier of sediment as it overflow during strong summer monsoons and typhoons.
High sediment supply produces sediment with coarser grain size and a higher organic content at both sites, and the sudden impact of typhoon Morakot produced 13-20 cm thick rapid accumulated deposits, characterized by coarsening-fining sequences. These were formed by hyperpycnal flows, probably originating from canyon overflows in the Gaoping- and the Kaohsiung Canyon.
The sediment shows a cyclicity that we suggest is a result of both the monsoon and occasional typhoons. Preservation of sediment and flood deposits is strongly reliant on the strength of the coming monsoon seasons and the occurrence of mass flows, which increases the energy at the locations and thereby the amount of erosion.

Acknowledgements

I would like to thank my supervisor Eve Arnold at IGV, Stockholm, for agreeing to help me with my writing and bringing structure back into my life; my supervisors Ludwig Löwemark and Chih-Chieh Su at NTU, Taipei, for having patience; Cheng YI-YA, Lin Chi-Yu, and YU-TUNG CHEN at the institute of Oceanography, NTU; and Magnus Mörth and Richard Gyllencreutz for their help on the ^{210}Pb interpretation.

Thank you David, Richard, David, Isabelle, Muhktar, Martin & Yvette at Green Peas; Friends at IGV; My family and of course - Martina, Livija, Jenny, Oskar, Francesco and Katja.

References

Allan, Rob., Lindesay, J. Parker, D. E. 1996. El Nino Southern Oscillation and Climatic variability. University of Michigan: CSIRO

Appleby, P.G. 2008. Three decades of dating recent sediments by fallout radionuclides: a review. *The Holocene* 18, 83-93

Azar, L. 2009. Cavitation in ultrasonic cleaning and cell disruption. Controlled Environments *via* "http://www.cemag.us/article/cavitation-ultrasonic-cleaning-and-cell-disruption. Acquired 2013-01-11.

California Analytical Services, *via* http://www.caslab.com/Forms Downloads/Flyers/FREEZE_DRYING_BRO_EMAIL.pdf. Acquired 2013-01-14

Carter, L., J. D. Milliman, P. J. Talling, R. Gavey, and R. B. Wynn. 2012. Near-synchronous and delayed initiation of long run-out submarine sediment flows from a record breaking river-flood, offshore Taiwan. *Geophysical Research Letters,* 39.

Chang, C. P., Angelier, J., Lee, T. Q., & Huang, C. Y. 2003. From continental margin extension to collision orogen: structural development and tectonic rotation of the Hengchun peninsula, southern Taiwan. *Tectonophysics* 361(1), 61-82.

Chang, C. P. 2004. *East Asian Monsoon* (Vol. 2). World Scientific Publishing Company

Cheng KS, Hou JC, Wu YC, Liou JJ. 2009. Assessing the impact of climate change on annual typhoon rainfall—a stochastic simulation approach. *Paddy and Water Environment* 7(4), 333–340.

Cheng, Y.-Y., Su, C.-C. 2012. Sediment-laden flow induced by submarine cable failures off southeastern Taiwan. *Poster from European Geosciences Union-General Assembly.*

Huh, C.-A.,, Zahnle, D. L., Small, L. F., & Noshkin, V. E. 1987. Budgets and behaviors of uranium and thorium series isotopes in Santa Monica Basin sediments. *Geochimica et Cosmochimica Acta*, *51* (6), 1743-1754**.**

Cilas Siret, "Laser Diffraction in five minutes", *via* http://www.particle-size-analyzer.co.uk/. Acquired 2013-01-13.

Dadson, S.J., Hovius, N., Chen, Y.G., Dade, W.B., Hsieh, M.-L., Wilett, S.D., Hu, J.-C. 2003. Links between erosion, runoff variability and seimicity in the Taiwan orogen, *Nature* 426, 648-651.

Flett Research *via* http://www.flettresearch.ca/Webdoc4.htm. Acquired 2013-01-11

Ge, X., Li, T., Zhang, S., & Peng, M. 2010. What causes the extremely heavy rainfall in Taiwan during Typhoon Morakot (2009)?. *Atmospheric science letters 11*(1), 46-50.

Heiri, O., Lotter, A.F., & Lemcke, G. 2001. Loss on ignition as a method for estimating organic and carbonate content in sediments: reproducibility and comparability of results. *Journal of Paleolimnology* 25, 101–110.

Hsu, H. H., Liu, C. S., Yu, H. S., Chang, J. H., & Chen, S. C. 2013. Sediment dispersal and accumulation in tectonic accommodation across the Gaoping Slope, offshore Southwestern Taiwan. *Journal of Asian Earth Sciences*.

Huh, C. A., Small, L. F., Niemnil, S., Finney, B. P., Hickey, B. M., Kachel, N. B., ... & Williams, P. M. 1990. Sedimentation dynamics in the Santa Monica-San Pedro Basin off Los Angeles: radiochemical, sediment trap and transmissometer studies. *Continental Shelf Research 10*(2), 137-164.

Huh, C. A., Chu, K. S., Wei, C. L., & Liew, P. M. 1996. Lead-210 and plutonium fallout in Taiwan as recorded at a subalpine lake. *Journal of Southeast Asian Earth Sciences 14*(5), 373-376.

Huh, CA., Lin, H.-L., Lin, S., Huang, Y.-W. 2009. Modern accumulation rates and a budget of sediment off the Gaoping (Kaoping) River, SW Taiwan: A tidal and flood dominated depositional environment around a submarine canyon. *Journal of Marine Systems* 76, 405–416.

Hüneke, H., & Mulder, T. 2011. *Deep-sea sediments* (Vol. 63). Elsevier Science.

Lee, I., Wang, Y. H., Liu, J. T., Chuang, W. S., & Xu, J. 2009. Internal tidal currents in the Gaoping (Kaoping) submarine canyon. *Journal of Marine Systems* 76(4), 397-404.

Liew, P.M., Kuo, C. M., Huang, S. Y. & Tseng, M. H. 1998. Vegetation change and terrestrial carbon storagein eastern Asia during the Last Glacial Maximum as indicated by a new pollen record from central Taiwan. *Global and Planetary Change* 16–17, 85–94.

Lin, C. Y., Hsu, H. M., Sheng, Y. F., Kuo, C. H., & Liou, Y. A. 2011. Mesoscale processes for super heavy rainfall of Typhoon Morakot (2009) over Southern Taiwan. *Atmospheric Chemistry and Physics Discussions 10*, 13495-13517.

Liu, C.-S., Lundberg, N., Reed, D.L. and Huang, Y.-L., 1993. Morphological and seismic characteristics of the Kaoping Submarine Canyon. *Marine Geology* 111, 93-108.

Liu, J.T., Lin, H.-L. 2004. Sediment dynamics in a submarine canyon: a case of river–sea interaction. *Marine Geology* 207, 55–81.

Liu, J. T., Lin, H. L., & Hung, J. J. 2006. A submarine canyon conduit under typhoon conditions off Southern Taiwan. *Deep Sea Research Part I: Oceanographic Research Papers 53*(2), 223-240.

Liu, J.-T., Liu, K-J., Huang, J.-C. 2002. The effect of a submarine canyon on the river sediment dispersal and inner shelf sediment movements in southern Taiwan. *Marine Geology* 181, 357-386.

Mulder, T., Migeon, S., Savoye, B., Faugères, J.-C. 2001. Inversely-graded turbidite sequences in the deep Mediterranean. A record of deposits from flood-generated turbidity currents? *Geo-Marine Letters* 21, 86–93.

Mulder,T., Syvitski, J. P.-M., Migeon, S., Faugères, J.-C., Savoye, B. 2003. Marine hyperpycnal flows: initiation, behavior and related deposits. A review. *Marine and Petroleum Geology*, 20, Issues 6–8, 861-882.

NASA. 2013. Hurricane archive available online.
http://www.nasa.gov/mission_pages/hurricanes/archives/2005/h2005_haitang.html
http://www.nasa.gov/mission_pages/hurricanes/archives/2009/h2009_Morakot.html

Acquired 2013-04-25

Ruiz Fernandez, A. 2007. Pb-210 chronology and trace metal geochemistry at Los Tuxtlas, Mexico, as evidenced by a sedimentary record from the Lago Verde crater lake. *Quaternary research* 67, 181-192.

Schulz, H. D., & Zabel, M. (Eds.). 2006. *Marine geochemistry*. Springer**.**

Syvitski, J. P.M. 2007. Principles, Methods and Application of Particle Size Analysis. *Cambridge University Press*. p. 16.

Tu, J. Y., Chou, C., & Chu, P. S. 2009. The abrupt shift of typhoon activity in the vicinity of Taiwan and its association with western North Pacific-East Asian climate change. *Journal of Climate* 22(13), 3617-3628.

Water Resources Agency, Ministry of Economic affairs, Taiwan. *Via* http://eng.wra.gov.tw/ct.asp?xItem=48142&CtNode=7674
Acquired 2013-03-06

Wohlfarth, B. "Coring with a Russian Corer" via http://people.su.se/~wohlf/russian_corer.pdf. Acquired 2013-01-10.

Wu, M. C., W. L. Chang, W. M. Leung. 2004. Impacts of El Niño–Southern Oscillation Events on Tropical Cyclone Landfalling Activity in the Western North Pacific. *J. Climate,* 17, 1419–1428.

Yu, H. S., Chiang, C. S., & Shen, S. M. 2009. Tectonically active sediment dispersal system in SW Taiwan margin with emphasis on the Gaoping (Kaoping) Submarine Canyon. *Journal of Marine Systems 76*(4), 369-382.

Yu, H. S., & Huang, Z. Y. 2006. Intraslope basin, seismic facies and sedimentary processes in the Kaoping Slope, offshore southwestern Taiwan.*Terrestrial, Atmospheric and Oceanic Sciences 17*(4), 659-677.

Figure 3. Picture modified from *http://en.wikipedia.org/wiki/File:XRFScan.jpg*. Acquired 2012-01-10

Appendix

Original data collected at the department of Oceanography at National Taiwan University, NTU, Taipei, Taiwan.

^{210}Pb data used for calculating sedimentation rates is highlighted with grey.

2009_L28

Depth (cm)	Grain size (μm)	Clay (%)	Sand (%)	Clay/sand	Water content (%)	LOI (%)	$^{210}Pb_{ex}$ (dpm/g)
0.5	14.9546333	24.1	11.8	2.04237288	39.93055556	4.000833507	17.0887128
1.5	28.38458	22.3	17.5	1.27428571	35.13513514		
2.5	50.51747	15.2	37.4	0.40641711	32.49158249	2.874251497	1.78175670
3.5	45.59853	18.2	29.4	0.61904761	29.65204236	3.074141049	2.54656569
4.5	64.49033	14.3	38.1	0.37532808	29.05092593	3.472222222	22.7926380
5.5	89.4483533	11.1	46.1	0.24078091	27.05882353	2.913800081	6.17035198
6.5	44.14384	17.2	27.4	0.62773722	26.22601279	3.066538091	12.8633287
7.5	124.887423	9.36	53.8	0.17397769	26.25454545		
8.5	73.8457766	18.3	40.4	0.45297029	24.20343137	3.053115851	13.5731018
9.5	56.3193266	19.2	36.9	0.52032520	24.00849858		
10.5	68.3564733	10	50.1	0.19960079	23.34328358	2.97029703	5.66726022
11.5	98.7074866	24.2	29.7	0.81481481	25.45227698	2.776848444	7.18101827
12.5	51.2138233	14.3	33.8	0.42307692	27.40649908	3.5500516	17.4521567
13.5	50.2631766	17.4	34.4	0.50581395	26.73417722	2.891096133	7.24121503
14.5	34.77406	20	22.8	0.87719298	26.70588235	4.321826583	10.4236526
15.5	36.5137766	21.4	24.2	0.88429752	26.00732601		
16.5	41.5607866	16.9	27	0.62592592	25.26595745	3.516933383	10.6615165
17.5	46.0316766	18.2	32.2	0.56521739	25.90497738		
18.5	42.4127366	17.4	28.8	0.60416666	27.98874824	3.695918725	1.14184678
19.5	54.8016066	13.2	40.2	0.32835820	26.15291262	2.635847526	1.51387227
20.5	42.1559266	17.5	29.2	0.59931506	24.70760234	3.868544601	4.30304506
21.5	53.0505	15	38	0.39473684	25.23419204	3.023804418	2.83797763
22.5	54.8283033	14.9	40	0.3725	25.42911634	2.760351317	2.15579917
23.5		18.6	28.6	0.65034965	26.08982827	4.77562783	1.87891808
24.5	54.4664133	14.6	36.7	0.39782016	23.95833333	2.845121218	
25.5	60.15483667	13.3	42.8	0.310747664	24.00803616	3.98962697	2.466198344
26.5	47.11666	17.3	33.1	0.52265861	24.88038278	2.890060535	2.273135955
27.5	54.87554333	15.1	39.3	0.384223919	24.69592808	3.887688985	1.291421569
28.5	50.93344333	18	38.4	0.46875	25.15262515	2.775101176	
29.5	56.28431333	14.4	40.9	0.35207824	24.29679922		
30.5	61.06585	11.6	42.8	0.271028037	23.78854626	2.529302899	
31.5	45.08072333	13.8	28.6	0.482517483	23.08083376		
32.5	45.54601	16	30.8	0.519480519	25.25252525	4.093211753	
33.5	34.22995667	15.2	20.1	0.756218905	15.61382598		
34.5	51.68892	14.3	38	0.376315789	22.61728395	2.746037597	

Depth (cm)	Grain size (µm)	Clay (%)	Sand (%)	Clay/sand	Water content (%)	LOI (%)	$^{210}Pb_{ex}$ (dpm/g)
35.5	53.71897333	15.4	39.7	0.38790932	22.01750345		
36.5	52.94853333	13	38	0.342105263	21.56439067	3.671363366	
37.5	50.95586333	15.4	36.9	0.417344173	22.99326774		
38.5	42.3289	20.3	28.6	0.70979021	22.34468938	2.843507656	
39.5	60.25765	13.1	43.4	0.301843318	19.85930736		
40.5	61.64636333	10.9	43	0.253488372	19.46902655	2.342786683	
41.5	70.38530667	10.3	45.9	0.224400871	18.85542169	2.608695652	2.550030726

2010_L28

Depth (cm)	Grain size (µm)	Clay (%)	Sand (%)	Clay/sand	Watercontent (%)	LOI (%)	$^{210}Pb_{ex}$ (dpm/g)
0.5	53.83609667	24.2	32.8	0.737804878	25.92779957	2.958076186	13.85333717
1.5	78.77066	20.7	46.2	0.448051948	23.9769821		
2.5	55.30751333	24.7	35	0.705714286	24.49682203	2.486187845	9.942524705
3.5	65.45461667	18.8	40.9	0.459657702	28.14837984		
4.5	38.12855	27.4	26.6	1.030075188	26.91677368	2.766169154	6.827691972
5.5	36.93698333	25.7	23.8	1.079831933	27.08492065		
6.5	38.13854	29.6	25.8	1.147286822	25.84267434		
7.5	42.23729	27.2	28.8	0.944444444	25.59610444		
8.5	47.97301333	23.6	32.3	0.730650155	24.50173603	2.635782748	4.718936727
9.5	49.4244	23.7	31.5	0.752380952	24.71269702		
10.5	45.79337667	25.6	31.4	0.815286624	23.77569922		
11.5	44.36668667	24.2	29.7	0.814814815	25.05543507		
12.5	50.25265667	23.5	34.4	0.683139535	24.996905	2.905027933	1.870588761
13.5	40.62398	27.6	27.2	1.014705882	24.22013513		
14.5	34.33924	31.9	22.3	1.430493274	25.4165089		
15.5	42.54636333	24.8	29.9	0.829431438	24.8154723		
16.5	41.49401	26.6	27.8	0.956834532	24.90006558	2.799132663	0.913549004
17.5	48.27721	24.7	34.8	0.709770115	23.53462821		
18.5	38.39523	27	24.9	1.084337349	24.07392197		
19.5	44.51277	22.5	29	0.775862069	25.82638302		
20.5	36.74277333	24.6	23.3	1.055793991	26.17601891	3.440731901	2.264995814
21.5	35.07025333	29.9	23	1.3	24.79362708		
22.5	47.63688333	19.6	32.5	0.603076923	23.56131968		
23.5	32.72464333	25.8	20.4	1.264705882	24.83501541		
24.5	42.77860667	22.3	27.2	0.819852941	24.23022748	2.978466492	1.28382104
25.5	49.38239333	20.6	33.2	0.620481928	23.33707338		
26.5	51.18606	20.5	33.7	0.608308605	22.66221976		
27.5	50.80692667	21.3	33.5	0.635820896	24.20575365		
28.5	44.16551333	22.4	29.6	0.756756757	24.86418104	2.726574501	0.394953619
29.5	37.04731667	24.2	23	1.052173913	24.72687263		
30.5	26.73033	25.6	16.8	1.523809524	24.7620943		
31.5	43.42599	20.5	26.1	0.785440613	25.37178172		

Depth (cm)	Grain size (µm)	Clay (%)	Sand (%)	Clay/sand	Water content (%)	LOI (%)	$^{210}Pb_{ex}$ (dpm/g)
32.5	50.35696667	22.2	32.3	0.687306502	23.45725785	2.507522568	0.20920821
33.5	37.87547	26	24.1	1.078838174	24.30023719		
34.5	31.09966	29	19.4	1.494845361	24.7802233		
35.5	40.31033	26.6	25.5	1.043137255	24.36508403		
36.5	55.19002667	20.3	37.3	0.544235925	22.84811278	2.790512258	0.432503428
37.5	46.63797667	21.8	31.7	0.687697161	22.30706327		
38.5	47.34415333	22.7	34.7	0.654178674	22.17605432		
39.5	60.33534	18.7	43.7	0.42791762	21.43731767		
40.5	46.42868333	21.8	33.1	0.658610272	21.94784148	2.612540193	0.392230048
41.5	45.25383667	23.4	32.9	0.711246201	23.13051239		
42.5	51.98781333	19.3	37.5	0.514666667	21.70767148		
43.5	50.1735	20.7	37.7	0.549071618	21.22626064		
44.5	62.33919667	16.6	44.7	0.371364653	20.84483471	2.988966901	0.119703587
45.5	53.09979	19.7	39.7	0.496221662	20.35601738		
46.5	45.65881667	20.8	33.4	0.622754491	21.11393396		
47.5	50.47195667	18.9	33.1	0.570996979	20.85892094		
48.5	37.45366333	24.1	23.5	1.025531915	20.72725726	2.938196555	
49.5	29.84375	28.7	19	1.510526316	22.35818672		
50.5	35.20676	22.9	21.8	1.050458716	24.81011093		
51.5	22.38371667	31.9	15.2	2.098684211	24.7325519		
52.5	28.40388667	31.7	17.8	1.780898876	26.7363723	2.974504249	
53.5	44.55135333	27.2	30.8	0.883116883	24.1331606		
54.5	42.36164333	26.2	27.8	0.942446043	21.87349507		
55.5	46.92237333	22.7	32.2	0.704968944	22.49660546		
56.5	51.66389	19.7	34.2	0.576023392	22.90523216		
57.5	43.63474333	23.8	29.7	0.801346801	22.38166552		
58.5	46.71928333	21.5	32.1	0.669781931	23.68241313		
59.5	49.32775	21.1	34.7	0.608069164	22.56887605		
60.5	46.47227	23	31	0.741935484	22.07447938		
61.5	52.2484	20	36.7	0.544959128	23.65396607		
62.5	44.42812333	24.6	31.2	0.788461538	22.22677531		
63.5	57.33789	19.9	40.5	0.491358025	22.16809961		
64.5	37.78463667	27.5	24	1.145833333	21.89291802		
65.5	40.72399333	23.2	26.7	0.868913858	22.71141622		
66.5	37.93162	24.7	24	1.029166667	23.14903014		
67.5	46.4364	24.2	31.8	0.761006289	24.86496833		
68.5	49.93441	22.1	31.5	0.701587302	23.9916519		
69.5	54.54846	21.6	34.6	0.624277457	24.23654975		
70.5	64.99932667	18.3	40.7	0.44963145	23.84221008		
71.5	45.69764333	29	29.5	0.983050847	22.73754183		
72.5	59.38481333	23.9	42.7	0.55971897	20.44209398		
73.5	62.90947333	20.5	42.2	0.485781991	21.07103759		
74.5	49.96488667	24.4	33.5	0.728358209	21.57908922		
75.5	69.95658667	16.4	48.3	0.339544513	21.32575778		
76.5	48.15213333	21.3	32.3	0.659442724	21.130811		

Depth (cm)	Grain size (µm)	Clay (%)	Sand (%)	Clay/sand	Water content (%)	LOI (%)	$^{210}Pb_{ex}$ (dpm/g)
77.5	44.80848333	24.9	30.6	0.81372549	23.03958626		
78.5	41.22223333	28.1	24.8	1.133064516	22.76811506		
79.5	44.32284333	31.3	24.7	1.267206478	24.21820239		
80.5	18.45750667	35.5	14.2	2.5	23.17955059		
81.5	42.40289	28.4	25	1.136	24.33437232		
82.5	45.97834333	28.4	29.8	0.953020134	24.04176088		
83.5	69.17362333	17.6	44.1	0.399092971	22.21583332		
84.5	51.31706667	25.4	32.5	0.781538462	21.34688		
85.5	46.69361333	23.2	32.7	0.709480122	22.08770134		
86.5	61.46897333	19.4	41.8	0.464114833	21.27291329		
87.5	67.42468667	15.7	46.1	0.340563991	21.00887731		
88.5	90.94406667	11	59.6	0.184563758	21.03158698		
89.5	69.71385	17.2	48.7	0.353182752	20.70520958		
90.5	88.01759333	14.3	55.2	0.259057971	21.82010348		
91.5	70.31311	17.7	46.1	0.383947939	21.05955288		
92.5	74.55904	16.1	48.4	0.332644628	21.18652589		
93.5	57.08634	22.6	37.6	0.60106383	20.89389702		
94.5	41.30353333	26.4	23.8	1.109243697	21.13684232		
95.5					23.79549222		
96.5					23.09182725		
97.5					21.33291358		
98.5					19.8201281		
99.5					19.39992728		
100.5					20.26145435		
101.5					19.62601154		

2009_L9

Depth (cm)	Grain size (µm)	Clay (%)	Sand (%)	Clay/sand	Watercontent (%)	LOI (%)	$^{210}Pb_{ex}$ (dpm/g)
0.5	16.51246333	17.7	1.8	9.833333333	32.29118059	4.223138873	3.766462988
1.5	16.24831333	18.2	1.4	13	33.67593712		
2.5	14.32297667	19.7	1.1	17.90909091	38.6036961	4.329371817	4.567107982
3.5	15.90076	17.2	2.6	6.615384615	39.90208078	4.704684318	29.67425099
4.5	11.83237333	20.7	0.7	29.57142857	39.01490603	4.622527251	32.09460414
5.5	8.468833333	26.2	0	∞	38.44919786	5.195827593	10.48967427
6.5	8.58118	25.8	0	∞	37.22570533	3.494623656	34.47955932
7.5	9.35056	24.6	0	∞	37.30534868	5.475853708	5.607757627
8.5	11.54918	21.4	1	21.4	37.83244681	4.347826087	17.17822751
9.5	15.26100333	18.9	2.9	6.517241379	37.76908023		
10.5	12.402	22.4	1.9	11.78947368	38.10096154	4.587712207	28.97284801
11.5	11.39175333	22.9	1.1	20.81818182	37.43932039		
12.5	17.34467333	17.5	5.3	3.301886792	34.63718821	4.62305774	26.74801283
13.5	16.05086	18.5	4.2	4.404761905	36.79508654		
14.5	17.51804333	17.6	5	3.52	36.71328671		

Depth (cm)	Grain size (µm)	Clay (%)	Sand (%)	Clay/sand	Watercontent (%)	LOI (%)	$^{210}Pb_{ex}$ (dpm/g)
15.5	14.11553667	20.2	2.4	8.416666667	36.53603034		
16.5	14.28166	20.5	3.4	6.029411765	36.64996421	5.216311323	29.0606348
17.5	12.25811667	23.1	2	11.55	36.54532477		
18.5	10.57591667	25.4	2	12.7	36.44214162	4.710144928	8.167463116
19.5	12.19991	23.7	3.1	7.64516129	36.65080052		
20.5	12.21047	22.4	2.1	10.66666667	36.51419558	5.047106326	21.30960504
21.5	11.58028	23.7	1.2	19.75	35.23622047		
22.5	11.53244333	23.2	1.6	14.5	35.71004159	5.328705594	13.10611452
23.5	11.61148333	24.1	2.7	8.925925926	34.76775956		
24.5	11.18260333	24	1.3	18.46153846	34.94913226	4.976978733	17.56711005
25.5	10.4624	25.2	0.8	31.5	35.17060367		
26.5	12.04174667	23	1.4	16.42857143	36.60565724	4.990833164	
27.5	11.35194667	23.4	1.1	21.27272727	37.27034121		
28.5	11.76893	22.9	1.1	20.81818182	35.95425304	4.773317356	7.522531635
29.5	10.51969	24	0.2	120	36.47798742		
30.5	12.63258333	21.5	2.5	8.6	35.62071117	4.626607794	
31.5	15.62937667	17.5	2.9	6.034482759	34.7799511		
32.5	13.91976	18.5	2.7	6.851851852	36.45833333	4.767812832	5.111718192
33.5	14.89171667	18.4	3.5	5.257142857	35.76826196		
34.5	9.97687	24.9	0.5	49.8	36.76293622	4.912898806	
35.5	8.409903333	28.1	0	∞	36.56927427		
36.5	9.969703333	25.1	0.002	12550	35.68281938	4.447574965	4.399807082
37.5	12.90546667	20.7	1.4	14.78571429	35.65957447		
38.5	10.14264333	24.5	0.6	40.83333333	35.87886768	4.709480122	
39.5	13.75790333	19	1.6	11.875	34.86725664		
40.5	10.95392333	23.7	0.7	33.85714286	32.74559194	4.571655734	0.950814733
41.5	12.66781	21.3	2.4	8.875	33.82352941		
42.5	11.53322333	22.8	0.9	25.33333333	32.9887218	4.294720252	3.36710638
43.5	15.03125667	20.2	3.2	6.3125	31.10047847		

2010_L9

Depth (cm)	Grain size (µm)	Clay (%)	Sand (%)	Clay/sand	Watercontent (%)	LOI (%)	$^{210}Pb_{ex}$ (dpm/g)
0.5	8.862796667	33.3	0.7	47.57142857	36.02411856	2.551665964	16.9560229
1.5	9.20586	31.7	0.6	52.83333333	37.43134709	2.346345515	17.80667333
2.5	9.327643333	33	0.6	55	38.07060649	3.395904437	23.13105707
3.5	10.72173667	30.3	1.5	20.2	38.60699547	4.3877144	25.42334706
4.5	11.40455333	30.1	1.9	15.84210526	38.53529621	3.126376046	22.77119963
5.5	11.31942333	30.1	1.2	25.08333333	38.28267979	4.44910808	25.22293621
6.5	12.21517667	29	2.1	13.80952381	37.09839417	3.378119002	18.35840433
7.5	11.62699667	29.1	1.6	18.1875	36.86634803	4.679410593	15.65639178
8.5	12.64264667	28.3	2.2	12.86363636	37.05302749	3.311258278	14.62989715
9.5	12.26606667	28.5	1.9	15	36.78195066	4.739548402	13.4442743
10.5	10.52200333	32	1.3	24.61538462	38.19344307	3.17364059	7.43348101
11.5	9.040296667	32.7	0.6	54.5	38.02274316	4.147936248	6.988146548
12.5	10.32621667	30.6	1.1	27.81818182	39.08854629	3.146430012	5.075664894
13.5	8.081283333	36.2	0.2	181	39.51009774	4.1352657	4.04442231

Depth (cm)	Grain size (µm)	Clay (%)	Sand (%)	Clay/sand	Watercontent (%)	LOI (%)	$^{210}Pb_{ex}$ (dpm/g)
14.5	10.7082	29.7	1.1	27	38.5277929	3.173652695	4.016179945
15.5	10.45029667	31.9	1.1	29	37.93035521	4.205046055	3.494647181
16.5	11.16325	30.5	1.4	21.78571429	37.15877798	3.318100536	3.010872927
17.5	10.67350333	31.7	1.2	26.41666667	36.81254123	4.179873217	2.663440845
18.5	12.30576	29	1.9	15.26315789	36.4632614	2.830005815	1.812178182
19.5	10.66414333	31.1	0.9	34.55555556	36.66422048		
20.5	13.43937333	28.2	2.8	10.07142857	37.35271367	3.048180924	1.369492013
21.5	10.46624333	31.5	1	31.5	36.69552126		
22.5	10.43445	31.2	0.8	39	37.06607347	2.771206489	0.600278412
23.5	7.229073333	39.8	0	∞	38.74409525		
24.5	10.36463	33.4	1.1	30.36363636	36.41524918	2.860207365	0.291892108
25.5	12.00752	29.2	1.9	15.36842105	35.83403236		
26.5	9.317176667	34.1	0.6	56.83333333	35.51124098	3.042479908	-0.060820271
27.5	12.41063667	29.4	1.8	16.33333333	33.02376419		
28.5	13.40735	27.7	3.2	8.65625	34.24734341	2.996845426	0.362383176
29.5	9.6327	34.1	1	34.1	35.5649496		
30.5	9.393213333	33.3	0.7	47.57142857	36.24009654	2.958349552	0.366322002
31.5	9.697696667	32.9	1	32.9	36.37576343		
32.5	7.501943333	36.4	0.001	36400	37.79599323	2.947113444	2.176865065
33.5	7.864036667	36.4	0	∞	38.99537484		
34.5	7.294596667	39.1	0	∞	35.01523973	4.087398757	2.264500637
35.5	7.185653333	39.9	0	∞	35.51135929		
36.5	6.294256667	41.7	0	∞	37.29324621	4.112918302	2.23366343
37.5	9.504396667	34.5	0.8	43.125	34.83440199		
38.5	9.277383333	35.2	0.4	88	34.71920719	4.357500464	
39.5	9.215543333	34.2	0.5	68.4	34.22623084		
40.5	11.80867667	29.8	2.1	14.19047619	34.03079178	4.370629371	1.927379381
41.5	9.756993333	33	0.7	47.14285714	34.58827807		
42.5	9.066913333	33.6	0.5	67.2	35.77561165	4.213536702	
43.5	9.817076667	33.2	0.6	55.33333333	33.6223118		
44.5	10.50451333	32.7	1	32.7	32.40754747	4.353157572	
45.5	13.54833333	28	2	14	30.15088096		
46.5	10.90826	30.8	1	30.8	33.01356342	4.267931239	
47.5	9.843536667	33.4	0.7	47.71428571	33.4239474		
48.5	10.00970667	33.3	0.8	41.625	37.76362503	4.438052188	
49.5	10.45528	31.5	1	31.5	32.40379284		
50.5	10.14112	32	1.2	26.66666667	34.1434274		
51.5	9.803123333	32.3	0.9	35.88888889	34.45718959		
52.5	10.93871333	30.4	1.7	17.88235294	34.99925383		
53.5	11.52354	30.1	2.3	13.08695652	34.76476862		
54.5	11.88262667	29.3	2	14.65	34.87830782		
55.5	12.05902667	29.3	2.2	13.31818182	34.66481417		
56.5	13.19499333	27.4	2.7	10.14814815	34.30876327		
57.5	10.58438333	30.7	1.2	25.58333333	34.01373937		
58.5	10.92811333	30.5	1.4	21.78571429	33.97465041		

Depth (cm)	Grain size (µm)	Clay (%)	Sand (%)	Clay/sand	Watercontent (%)	LOI (%)	$^{210}Pb_{ex}$ (dpm/g)
59.5	10.4093	31.2	1.1	28.36363636	33.72424407		
60.5	13.53924667	26.9	2.7	9.962962963	33.80185035		
61.5	11.94088667	29.2	1.8	16.22222222	34.38236883		
62.5	13.38241333	27.4	2.6	10.53846154	34.11444347		
63.5	14.25978	26.5	2.6	10.19230769	32.93442142		
64.5	12.26073667	28.1	1.7	16.52941176	34.82724042		
65.5	11.09978	31.1	1.5	20.73333333	34.67111459		
66.5	10.77534667	30.5	1.2	25.41666667	58.16702052		
67.5	9.72764	32.7	0.8	40.875	35.80949451		
68.5	9.131043333	33.6	0.6	56	35.76339527		
69.5	9.046306667	33.6	0.6	56	35.45418623		
70.5	7.89107	36.1	0.001	36100	35.22629333		
71.5	9.93933	32.9	1.1	29.90909091	34.25011924		
72.5	13.05511667	28.4	2.5	11.36	34.12680026		
73.5	9.47707	33.8	0.9	37.55555556	33.62112722		
74.5	13.79510667	28.3	3.6	7.861111111	33.80780739		
75.5	13.80249667	28.1	3.5	8.028571429	33.48309618		
76.5	13.16025667	29.1	2.9	10.03448276	34.14161907		
77.5	12.19953667	30	2.5	12	32.95770333		
78.5	12.68548667	28.4	2.3	12.34782609	32.84982935		
79.5	11.63830333	29.6	1.2	24.66666667	34.21965552		
80.5	14.17887667	26.6	3	8.866666667	33.996876		
81.5	13.07342667	29.8	3.1	9.612903226	34.4917816		
82.5	13.17518	29	2.4	12.08333333	33.7791708		
83.5	10.28502667	33.1	1.1	30.09090909	32.7772386		
84.5	13.71642333	27.7	2.6	10.65384615	31.69982078		
85.5	15.40447	26	2.6	10	29.78409941		
86.5	12.98585	30.6	2.4	12.75	31.65260217		
87.5	8.688763333	36.6	0.5	73.2	34.16913054		
88.5	8.038866667	37.2	0.003	12400	34.44359949		
89.5	12.11224	30.6	2.3	13.30434783	33.43223117		
90.5	15.48129	27.2	3.9	6.974358974	30.81791194		
91.5	18.52406667	26	6.3	4.126984127	28.95475049		
92.5	17.23993333	28	6.2	4.516129032	32.75086273		
93.5	10.67321667	31.1	1.2	25.91666667	34.55533862		
94.5	10.83098667	31	1.1	28.18181818	33.97871158		
95.5	11.56941333	29.9	1.8	16.61111111	34.21579813		
96.5	10.46754667	31	0.9	34.44444444	32.41381398		
97.5	10.16211667	32.7	0.8	40.875	31.62031829		